COMMUNICATIONS IN SCIENCE AND TECHNOLOGY
Homepage: cst.kipmi.or.id

Hybrid-intelligent P&O-InC algorithm with deterministic adaptive weighting for maximum power point tracking under dynamic conditions

Devi Handaya[a,b,*], Nevra Bayhan[a], Bernadeta Siti Rahayu Purwanti[c], Hasvienda Mohammad Ridlwan[d]

[a]*Department of Electrical and Electronics Engineering, Istanbul University-Cerrahpasa, Istanbul 34320, Türkiye*
[b]*Department of Mechanical Engineering, Politeknik Negeri Jakarta, Depok 16425, Indonesia*
[c]*Department of Electrical Engineering, Politeknik Negeri Jakarta, Depok 16425, Indonesia*
[d]*Department of Electrical Engineering, Universitas Indonesia, Depok 16424, Indonesia*

Article history:
Received: 21 November 2025 / Received in revised form: 17 December 2025 / Accepted: 18 December 2025

Abstract

Electricity generation remains dominated by fossil fuel–based sources, underscoring the necessity to optimize the utilization of solar energy through photovoltaic (PV) systems in support of the Sustainable Development Goals (SDGs). Variations in solar irradiance and temperature significantly influence PV performance, necessitating effective Maximum Power Point Tracking (MPPT) methods. This present study proposes HI-POnIC as an adaptive development of conventional MPPT algorithms using a deterministic, feature-based decision mechanism. The method employed dynamic weighting and adaptive step adjustment to modify the control response to changes in PV operating characteristics, without any reliance on learning processes. Performance of the system was evaluated through convergence analysis, energy and power tracking efficiency, and spatial accuracy assessment. The findings from the simulation demonstrated that HI-POnIC achieved faster convergence and enhanced stability around the maximum power point when compared with conventional methods. Its lightweight and easily implementable adaptive structure has rendered HI-POnIC suitable for PV systems operating under dynamically varying environmental conditions.

Keywords: Photovoltaic; maximum power point tracking; hybrid MPPT algorithm; adaptive feature-based control; energy efficiency

1. Introduction

Electricity is regarded as one of the most pivotal sources of energy used in many aspects of daily life, including lighting, transportation and industrial processes. It is an important energy source that propel economic and social growth on a global basis. In 2019, the International Energy Agency (IEA) released data concerning the global generation of electricity based on the types of energy used. Most electricity is still generated from conventional sources, such as coal (36.7%), natural gas (23.6%), hydropower (15.7%), nuclear (10.7%), non-hydro renewable energy and waste (10.8%), and oil (2.8%) [1]. From this data, despite the finite nature of coal as an energy source and its environmental impacts, it continues to predominate global electricity generation. Coal combustion produces elevated carbon emissions that contribute to global warming and air pollution [2]. As these natural resources are limited and detrimental to the environment, there is a need for alternative solutions that are both cleaner and more sustainable to meet the requirement of future electricity. Renewable energy, particularly solar power from natural sources, is a better alternative for the environment [3]. The transition to renewable energy is dependent upon the realization of "Affordable and Clean Energy," in line with the Sustainable Development Goals (SDGs) aimed at ensuring universal access to affordable, accessible, and long-lasting energy in both developed and developing countries [4].

Solar energy is one of the most promising types of renewable energy. The process of its conversion into electrical energy is performed through photovoltaic effect using photovoltaics (PV) [5,6]. In PV systems, electricity is generated when light hits semiconductor materials such as silicon. In this process, the photons in the light make an electric current by hitting electrons out of the atoms in the semiconductor material.

Many studies have been conducted on the subject of PV systems. Lüer L. et al. examined sophisticated photovoltaic architectures, including multi-junction cells and multi-excitation generation, to surpass the efficiency constraints of individual cells and attain enhanced power conversion efficiency [7]. Dada M. et al. examined the latest developments in solar photovoltaic materials and systems for multi-

* Corresponding author
Email: devi.handaya@ogr.iuc.edu.tr
https://doi.org/10.21924/cst.10.2.2025.1840

generation applications, with an emphasis on the enhancement of the performance and efficiency of PV systems [8]. Hossain et al. conducted a study into the management of photons in silicon photovoltaic cells to reduce optical losses and enhance the efficiency of the power conversion process. The study examined surface texture and nanostructure as potential solutions [9]. Mulda et al. highlighted that enhancements in solar cell efficiency remain predominantly influenced by the capacity of system to optimally extract available electrical energy [10].

Rihani A.T. and Ghandchi M. suggested a solution using methods to monitor the energy requirement for PV systems to function optimally [11]. The method employed in this study is unique since the proposed algorithm has been designed to generate electrical energy that can be utilized to track processes that are like those of PV modules.

Maximum Power Point Tracking (MPPT) is a technique employed in photovoltaic systems to ensure that solar power systems operate at maximum power points under various environmental conditions. This technique is employed to optimize the conversion of solar energy from solar panels into electrical energy [12]. The MPPT method utilizes a voltage-current (V-I) curve to maximize electrical power output. Haque A. proposed a solution for the MPPT scheme to enhance the speed and accuracy of maximum power tracking in stand-alone and grid-connected photovoltaic systems, particularly in areas with rapid changes in solar radiation [13]. Samosir A.S. and others utilized a number of hybrid methods, including fuzzy-neural MPPT optimized with genetic algorithms, to examine the efficacy of Maximum Power Point (MPP) tracking in different atmospheric and load conditions for the enhancement of performance [14]. Ali A. et al. introduced a hybrid approach that integrates a conventional MPPT, specifically the Perturbation and Observation (P&O) method, with fuzzy logic controllers. The results of the simulation demonstrated that the output voltage could stably be reversed [15].

The P&O and Incremental Conductance (InC) are foundational MPPT methods for PV modules, frequently conducted in combination with other methods [12,13,15,16]. Yuksek et al. created a hybrid algorithm utilizing different step sizes to reduce oscillations and speed up MPP tracking [17]. Bhat et al. integrated P&O and InC employing Fibonacci theory and the golden ratio, resulting in an enhanced performance under partial shading and varying environmental conditions [18]. Neeraj et al. proposed a novel integration of a Cuk–SEPIC hybrid converter with a gravitational search algorithm-particle swarm optimization (GSA–PSO) hybrid MPPT algorithm in a photovoltaic system for water pumps [19].

The P&O and InC methods are characterized by ease of implementation, owing to their independence from complex computational requirements. The MPPT method, in common with many researchers, is frequently implemented in conjunction with the algorithms of artificial intelligence (AI). However, the implementation of MPPT method, when applied with AI algorithms, requires complex computations. Therefore, development is required to ensure that the P&O and InC algorithms can still be utilized, with results that can still track the maximum power point.

This present study proposes an algorithm for the development of a combination of the P&O and InC algorithms. It is expected to yield results that can achieve the maximum power point. The proposed algorithm will not utilize AI algorithm integration, but it will create an AI-inspired algorithm that can adapt effectively to both static and dynamic environments. The algorithm will be analyzed based on its convergence capability in tracking the maximum power point (MPP), tracking efficiency, and power loss, as well as spatial and statistical analysis of power tracking accuracy.

2. Materials and Methods

PV modules refer to a system utilized as a source of renewable energy. The utilization of sunlight, when naturally generated, has the potential to produce electrical energy. The widespread utilization of electrical energy processed from environmentally unfriendly and finite energy sources is undoubtedly a serious concern, thus rendering it one of the SDGs goals.

MPPT, a method for maximizing energy efficiency, is expected to contribute to the realization of the SDGs. The P&O and InC methods are commonly used due to their ease of application in PV systems. However, these methods still have weaknesses, particularly in terms of the determining factors of energy produced by PV, namely solar irradiation and temperature.

The PV system can be modeled using an equivalent circuit consisting of a current source, diodes, and resistors connected in series and parallel. The output current (I) from the solar cell is shown in Eq. (1) [20].

$$I = I_{ph} - I_s\left(e^{\frac{V+IR_S}{n\frac{kT}{q}}} - 1\right) - \frac{V+IR_s}{R_{sh}} \quad (1)$$

where I_{ph} is the photogenerated current that depends on irradiance (G) and temperature (T). The diode current follows the Shockley equation to describe the current and voltage characteristics of semiconductor diodes, including photovoltaic diodes [21]. I_S is defined as the reverse saturation current, which is the current that flows through the diode when the voltage is applied in the opposite direction (reverse bias). The solar cell creates V, which is defined as the voltage. n is the ideality factor, which is a measure of the energy changes and the functionality of semiconductor devices system. Number n is typically situated within the range of 1 and 2. A value of 1 indicates a perfect system. Higher values mean that greater number of losses in the system. The Boltzmann constant, k, equals 1.38×10^{-23} J/K. It demonstrates a correlation of temperature and energy on a small scale, like in semiconductor systems. The solar cell works at a temperature of T, and the charge of the electron is q (1.602×10^{-19} C). Meanwhile, R_s represents the series resistance, and R_{sh} represents the shunt resistor, which determines the current path through the lower resistance rather than through the main load. The MPPT will process all quantities that yield an output current from the PV.

2.1. Maximum Power Point Tracking (MPPT) Algorithm

MPPT controls current and voltage to obtain maximum

power output. The P&O algorithm is responsible for the monitoring of the power generated by the system by adjusting the output voltage of the PV panel in small increments. If the power increases because of the alteration, the modification will continue in the same direction; otherwise, the direction of the change will be reversed. This cyclic process enables the system to reach its maximum power point.

P&O utilizes Eq. (2-4) for voltage distortion. The difference is attributed to variations in step size associated with either fixed or variable duty cycle settings. After monitoring the PV power ($P(t)$), the power difference (ΔPV) is obtained by comparing it with the previous maximum power ($P(t-1)$). The ΔPV is utilized to calculate the duty ratio, which, in turn, regulates the converter to increase or decrease the voltage ($V(t)$) depending on the voltage difference (ΔV) [22].

$$P(t)=V(t)\ x\ I(t) \tag{2}$$

$$\Delta PV=P(t)\ -\ P(t-1) \tag{3}$$

$$V(t)=V(t-1)\pm\Delta V \tag{4}$$

Meanwhile, the InC algorithm continuously monitors and analyzes voltage and current values to obtain the maximum power that can be generated by the panel. This is because the slope of the PV array power curve is zero at the maximum point (MPP). In the InC MPPT algorithm, the terminal voltage system is constantly set to the PV voltage at the MPP. It is based on the increase in conductivity of the PV array. The operation of the InC MPPT technique is predicated on the premise that the derivative of power with respect to voltage is zero at the MPP, as expressed in Eq. (5).

$$\frac{dP}{dV}=I+V\frac{dI}{dV} \tag{5}$$

When the derivative of power with respect to voltage is zero at the maximum power point, i.e., dP/dV=0, Eq. (5) can also be expressed as follows.

$$I+V\frac{dI}{dV}=0 \tag{6}$$

Equivalently, Eq. (6) can be written as follows [23].

$$\frac{dI}{dV}=-\frac{I}{V} \tag{7}$$

In this context, dI/dV signifies the additional conductivity, while I/V represents the instantaneous conductivity.

P&O is fast in processing its algorithm towards stability, yet it is not readily stable. In contrast, InC can be more accurate in terms of stability, though its responsiveness is not as expeditious as that of P&O, thereby leading to the identification of weaknesses in both algorithms. For this reason, this study will combine P&O and InC into Hybrid P&O and InC (H-POnIC). The H-POnIC algorithm used in this study does not merely combine the two. The H-POnIC algorithm does not employ ON/OFF logic, where one is turned on and the other is turned off.

In the H-POnIC algorithm, changes in the duty cycle of the converter are determined by considering the contributions of P&O and InC. The primary objective of this approach is to utilize the fast response advantage of P&O while maintaining the stability and accuracy of InC around MPP. Changes in the duty cycle (ΔD) are formulated as a weighted combination of two correction signals generated by the P&O and InC algorithms.

$$\Delta\mathrm{D}=\omega_{po}\Delta D_{po}+\omega_{inc}\Delta D_{inc} \tag{8}$$

The weight values of the P&O (ω_{po}) and InC (ω_{inc}) algorithms are adaptively determined based on the strength of information provided by each method. The P&O method provides information through the power gradient with respect to voltage, while the InC method provides information through the incremental error between dI/dV and -I/V. Both demonstrate the sensitivity of the system to the operating position relative to the MPP point.

The weight ω_{po} is calculated using the following equation.

$$\omega_{po}=\frac{|\mathrm{dP}/dV|}{|\mathrm{dP}/dV|+|(\mathrm{dI}/dV)+I/V|} \tag{9}$$

The ω_{po} weight is indicative of the change in power relative to the voltage applied, which is utilized to evaluate the dominant dynamics and incremental errors. When the P&O gradient increases due to rapid changes in solar irradiation or temperature, the ω_{inc} weight will increase, rendering the algorithm more responsive to changes. Conversely, when the system is near MPP, the weight ω_{po} will be greater, causing the system to be more stable and reducing oscillations around the optimal operating point, which can be expressed as follows.

$$\omega_{inc}=1-\omega_{po} \tag{10}$$

The H-POnIC algorithm can be developed to facilitate not only the examination of the gradient magnitude but also the rapid calculation of the power change. It can anticipate rapid changes in solar irradiation or temperature. If light conditions change quickly, the P&O weight automatically increases. Conversely, if conditions remain stable, the InC weight will increase. In essence, the H-POnIC algorithm also needs to adapt quickly. For the adjustment of an algorithm, additional intelligent methods, in general, are required. However, in this study, the HI-POnIC algorithm is an H-POnIC algorithm with an adaptive weighting mechanism inspired by several AI methods without using fuzzy logic, neural networks, PSO, or other AI methods. The adaptive weighting mechanism in HI-POnIC is a feature-based deterministic decision rule that adjusts the contribution of P&O and InC contextually. Since this approach does not involve data-based learning, it is more appropriately classified as an AI-inspired adaptive mechanism or heuristic inference layer. The concept of the weighting mechanism can change contextually based on local data characteristics, with the aim of enhancing accuracy and computational efficiency without the necessity of data-based learning [24].

In HI-POnIC, the ω_{po} and ω_{inc} weights are no longer dependent solely on the gradient magnitude, but also on the sensitivity function to map the system's dynamic level, as expressed in the following equation. Each variable has an ε_V as a tolerance threshold to prevent division by zero or minimal values in the variables V or ΔV. $\emptyset_3$ is also limited to a maximum

of 1.0; therefore, when its value is elevated, it is restricted to the range of 0 to 1.

$$\phi_1 = \frac{|dP|}{|dV|+\varepsilon_V} \quad (11)$$

$$\phi_2 = |e_{inc}| = \frac{dI}{|dV|+\varepsilon_V} + \frac{I}{V} \quad (12)$$

$$\phi_3 = min\frac{|dP|}{|P|+10^{-12}}, 1.0 \quad (13)$$

Each represents the sensitivity of the power-voltage gradient, the distance to the MPP, and the relative change in power. All three are used to calculate adaptive weight:

$$\omega_{po} = \frac{\emptyset_1}{\emptyset_1+\emptyset_2+\emptyset_3} \quad (14)$$

$$\omega_{inc} = \frac{\emptyset_2}{\emptyset_1+\emptyset_2+\emptyset_3} \quad (15)$$

In addition to the dynamic gain factor $g = \emptyset_3$, the duty cycle change step is automatically adjusted using the following equation.

$$step = step_{min} + g(step_{max} - step_{min}) \quad (16)$$

Subsequently, the combined voltage command (V_{cmd}) is calculated as follows.

$$V_{cmd} = \omega_{po}V_{po} + \omega_{inc}V_{inc} \quad (17)$$

Based on the flow described above, the HI-POnIC algorithm can be formed with the flowchart as presented in Fig. 1.

2.2. Research Methodology

HI-POnIC algorithm, as proposed in this study, will undergo evaluation in a static environment with solar irradiation and temperature inputs in accordance with the Standard Test Conditions (STC) commonly used in PV modules, namely 1000 W/m² and 25°C. The PV module employed in this study is of the monocrystalline variety and its specifications are outlined in Table 1 [25].

Table 1. PV module specifications

Specification	Value
Nominal Maximum Power	375.43W
Optimum Operating Voltage (V_{mp})	39.77V
Optimum Operating Current (I_{mp})	9.44A
Open Circuit Voltage (V_{oc})	48.45V
Short Circuit Current (I_{sc})	9.96A

To observe the response of PV under real conditions, dynamic testing was conducted using a PT100 RTD temperature sensor and a pyranometer solar irradiation sensor. Real-time condition testing can provide sufficient operational understanding to detect inefficiencies due to environmental factors such as clouds or weather variations [26,27].

As demonstrated in Fig. 2, the temperature sensor was attached to the PV, given that PV performance is also influenced by temperature [28–31]. In conditions of elevated temperature, for example, on a particularly hot day, the efficiency of the PV system can be significantly reduced. The pyranometer sensor was placed close to the PV module. Dynamic testing was carried out for approximately 33 minutes, and the results will be plotted in a graph for 20 seconds. Every 1 second represents hundreds of real conditions.

In addition to the measurements of temperature and solar radiation, electrical measurements are also taken using a PZEM-017 sensor. The ESP32 acquires data from the sensor and then transmits it via the Message Queue Telemetry Transport (MQTT) protocol to the server. The monitoring dashboard will display the data that is stored on the database server. This will enable users to observe the PV measurement conditions in real time, as illustrated in Fig. 3.

Researchers can use this monitoring dashboard to oversee how PV modules system works. The system displays solar irradiation and module temperature inputs, as well as module current and voltage outputs. The monitoring dashboard also has graphs that describe the performance of the PV modules, thereby facilitating the determination of the PV system's operational functionality.

To simplify the analysis process, a series of tests were conducted in the MATLAB environment. All tests were subsequently compared to determine the output power generated by all MPPT algorithms designed according to Fig. 4. The data obtained from the pyranometer and the RTD PT-100 were entered into the PV module. DC Chopper is a device that facilitates the conversion of the output of the PV module into a power converter. It is a power regulator that receives a control loop from the MPPT algorithm, allowing it to produce maximum power points. Subsequent to this, the MPPT algorithm will provide a control loop to the DC Chopper by processing the duty cycle (D) during a specific pulse period (P). The control loop is created using a Pulse Width Modulation (PWM) generator.

In this study, the PV module is constructed with one series (N_S) and two parallel (N_p) modules, enabling the total voltage (V_{Total}) to be calculated using equation below.

$$V_{Total} = N_S x V_{mp} = 1\ x\ 39.77 = 39.77V \quad (18)$$

Eq. (19) yields the total current (I_{Total}) from two parallel modules as follows.

$$I_{Total} = N_p x I_{mp} = 2\ x\ 9.44 = 18.88A \quad (19)$$

From Eq. (18) and (19), the following total power (P_{Total}) equation is derived.

$$P_{Total} = V_{Total} x I_{Total} = 39.77\ x\ 18.88 = 750.8576 \quad (20)$$

Eq. (20) demonstrates the total power that can be extracted from the PV module when controlled by the MPPT algorithm.

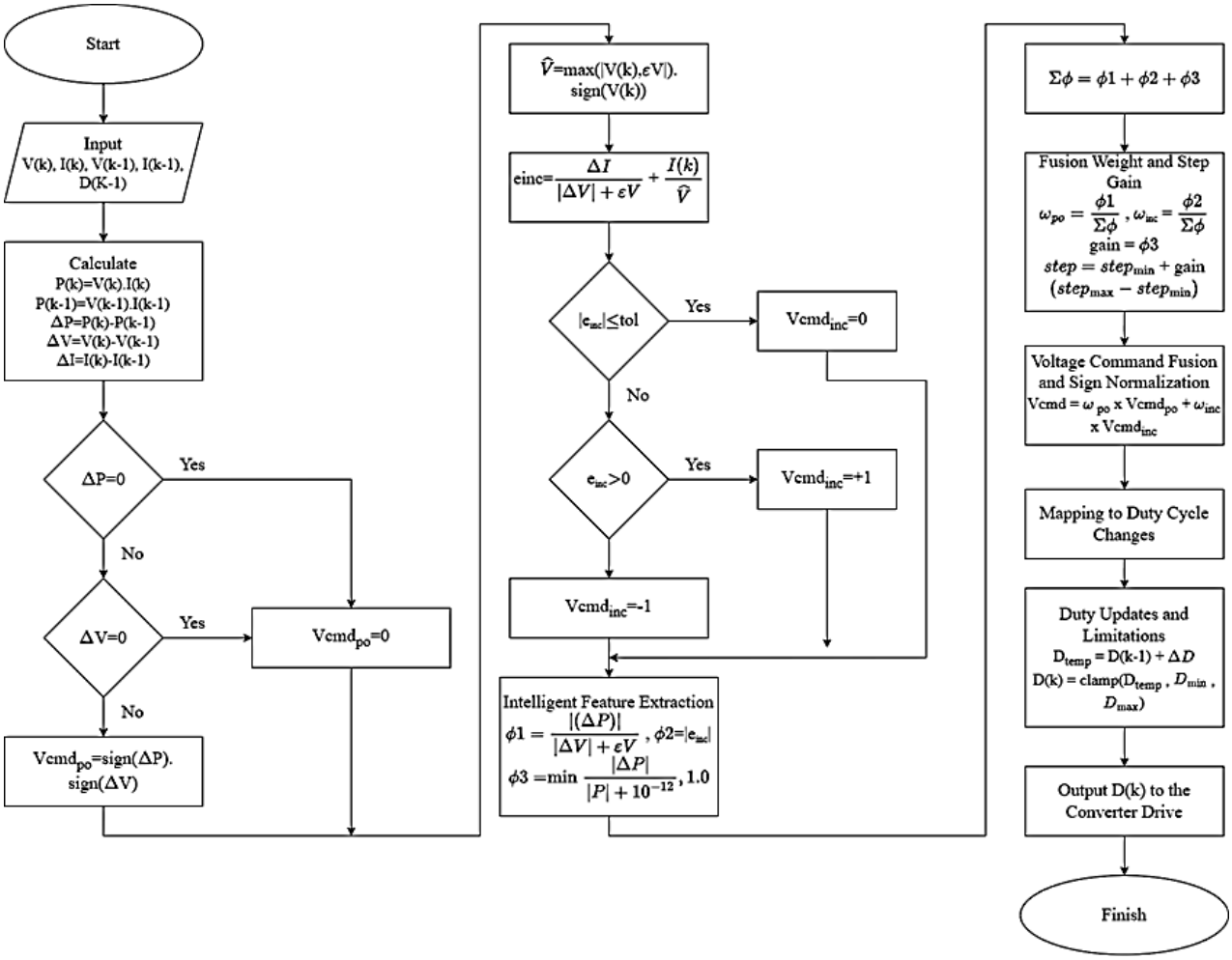

Fig. 1. Flowchart of the HI-POnIC algorithm

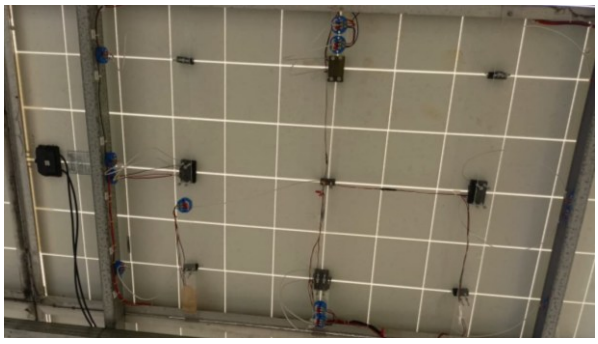

Fig. 2. Installation of PT100 RTD on PV module

Fig. 3. PV module real-time monitoring system

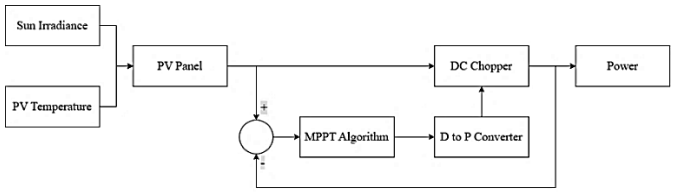

Fig. 4. Block diagram of MPPT algorithm testing on PV modules

3. Results and Discussion

The test results obtained from the four algorithms will be evaluated to assess the system's ability to quickly, efficiently, and accurately attain the maximum power point under various operating conditions. The analysis includes convergence response to environmental changes, tracking efficiency and power loss, as well as spatial and statistical mapping that shows the consistency and precision of the algorithm in following the maximum power point.

3.1. Power tracking dynamics/convergence

3.1.1. Static testing in the STC environment

Static testing is performed to assess the algorithm's capacity to attain the maximum power point under STC conditions. In accordance with the MPPT algorithm test design block as

depicted in Fig. 4, the control loop will continue to operate until attains the maximum power value, as indicated by the Voltage-Current (V-I) and Voltage-Power (V-P) curves as depicted in Fig. 5.

Test results under STC conditions demonstrate the transient and steady-state behavior of four algorithms: P&O, InC, H-POnIC, and HI-POnIC. The reference line of 750.8576 W is employed as the model-based maximum power reference, obtained from the PV characteristic calculation in Eq. (20), also illustrated in Fig. 5, and calibrated against the datasheet parameters (V_{oc}, I_{sc}, V_{mp}, I_{mp}) shown in Table 1. Accordingly, this reference value represents the computational upper limit for the purpose of simulation benchmarking, not empirical verification that the physical module necessarily achieves this value at STC.

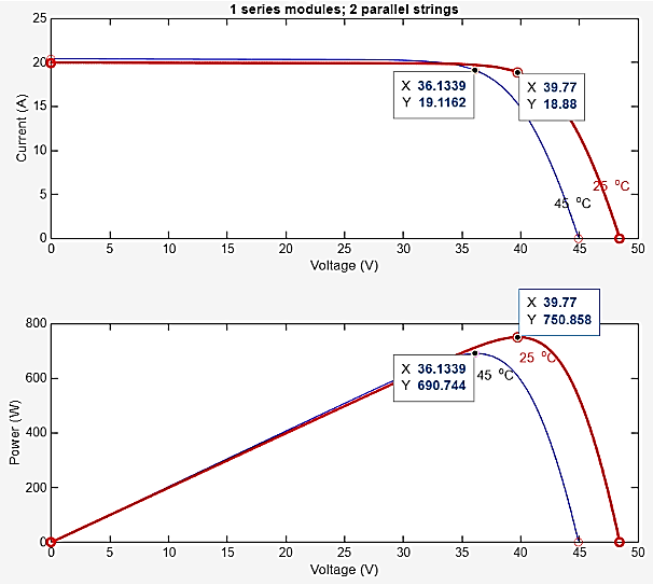

Fig. 5. V-I and V-P curves on the PV module

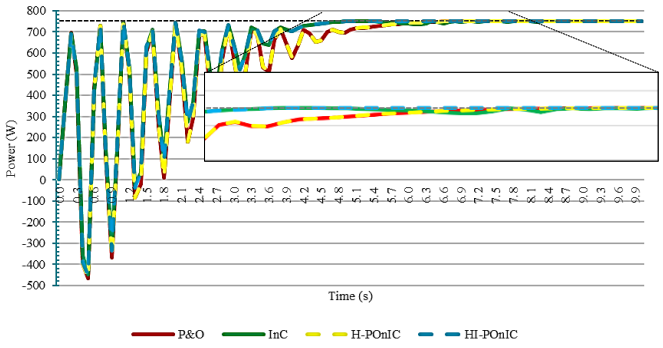

Fig. 6. Results of static testing in an STC environment

In the initial phase (t<4s), all algorithms demonstrate the oscillatory response that is characteristic of the P&O and InC methods. This is because they are searching for the direction of the power increase. However, when steady state conditions are reached, differences start to show up. It is important to consider the broader context in Fig. 6. The HI-POnIC curve clearly reaches the maximum power band with the greatest rapidity, while also exhibiting stability (t≈4.4s). InC is the next element to be considered, and P&O and H-POnIC require a longer time (t≈6.4s) to reach a stable state. InC, on the other hand, demonstrated an initial stability, subsequently exhibiting fluctuations at several t values prior to attain a stable state at t≈6.9s.

The HI-POnIC curve attains the maximum power band and demonstrates stability more rapidly, followed by InC. P&O and H-POnIC require longer periods to attain a stable state. This phenomenon is consistent with the core principle that adaptive step adjustments in HI-POnIC diminish the amplitude of oscillations as the power gradient relative to voltage (|ΔP|/|P|) declines. Thus, the step adaptation that HI-POnIC must perform accelerates the transition from the exploration phase to the stabilization phase.

Theoretically, the MPP condition can be expressed as the derivative of power with respect to voltage, dP/dV = 0, which can be decomposed into incremental conductance and instantaneous conductance. This relationship explains why power gradient-based and conductance-based decision directions can be consistent in determining the operating side relative to the MPP. However, the equivalence of these sign directions is inadequate to fully explain the similarity of dynamic responses. In the tests conducted, H-POnIC employed a combination of P&O and InC with relatively static/limited weight changes, and the test profile did not involve partial shading or truly extreme irradiance changes. Under conditions of smooth gradient changes and low measurement noise, the P&O component tends to dominate the correction decision, resulting in the transient response of H-POnIC appearing almost identical to P&O.

The practical consequence is that, while the direction of the mathematically derived sign may indicate a similar direction of correction around the MPP, the real-time response is determined by the discrete implementation, the perturbation step size, and the quality of the gradient estimation. P&O causes oscillations because of continuous fixed perturbations that reverse direction around the power peak. At the same time, InC is contingent on the ΔI/ΔV ratio, consequently rendering its performance susceptible to measurement noise and minor ΔV conditions. In this study, the combined strategy in H-POnIC does not significantly alter the perturbation step mechanism under STC conditions, so the oscillation pattern and settling time follow the characteristics of P&O.

Conversely, the similarity between InC and HI-POnIC occurs because the adaptive weighting mechanism in HI-POnIC tends to increase the contribution of the InC branch when the conductance error indicator is in a small range (i.e., the system is approaching a dP/dV ≈ 0 condition), so that the correction decision follows the character of InC. The distinguishing feature of HI-POnIC is its ability to enhance the signal-to-noise ratio in addition to increasing the gain. Instead, it adjusts the contribution of each branch contextually based on dynamic indicators such as |dP/dV|, $|e_{inc}|$, and relative power change |dP/P|. Therefore, residual oscillations around the MPP can be suppressed without eliminating the sensitivity of InC to changes in operating conditions.

The momentary instability in the InC curve after approximately 6 s can be attributed to the approach of ΔV to zero. This results in a heightened sensitivity of the ΔI/ΔV ratio to noise and quantization, thereby causing the I–V slope estimates to oscillate and reverse the duty cycle decision,

despite the actual operating conditions already close to MPP. HI-POnIC mitigates the effects of instability because adaptive weighting reduces the contribution of the InC branch when the gradient indicator is unreliable (e.g., ΔV is very small or power fluctuations are relatively high) and increases the role of the P&O branch, which is more stable against noise. As a result, the combined decision signal remains smooth and is not easily reversed.

Testing under real-time conditions is necessary, given the assumption that the system was stable under STC conditions. This is also evident from the V-I and V-P curves as depicted in Fig. 5, which demonstrate that both solar irradiation and temperature affect the maximum power output of the PV module. Therefore, dynamic testing is required to assess the robustness of the HI-POnIC algorithm in maintaining its maximum output.

3.1.2. Dynamic testing in a real-time environment

Dynamic testing was conducted under fluctuating conditions of sun irradiation and temperature, as illustrated in Figs. 7 and 8. The primary objective of this study was to assess the MPPT algorithm's capacity to adapt to rapid environmental changes and to measure the power output response of the photovoltaic system to these variations in input.

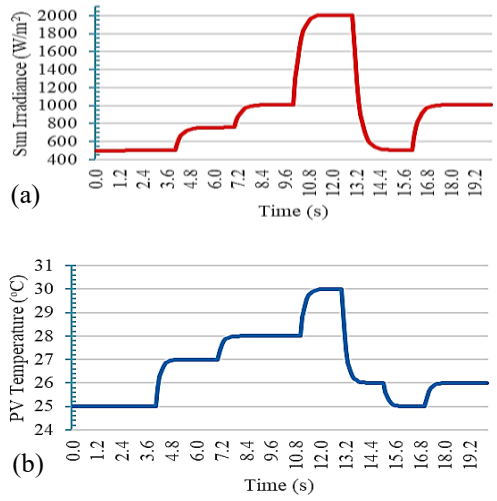

Fig. 7. (a) Sun irradiance and (b) PV temperature input in the real-time system

In depicted in Fig. 7(a), the initial irradiation intensity is approximately 500 W/m². The process undergoes a series of stages of increase until reaching 2000 W/m² at around t = 11 s, before decreasing dramatically to approximately 500 W/m² at around t = 13 s and returning to stability at approximately 1000 W/m² after t = 17 s. This pattern resembles fast-moving clouds or sudden weather changes in the field, which is one of the main challenges in MPPT system design. An increase in irradiation raises the maximum power, while a decrease in irradiation leads to a reduction in power. Therefore, it is imperative that the MPPT algorithm is capable of adjusting the operating point for each change to remain around the MPP.

As illustrated in Fig. 7(b), the temperature profile undergoes a simultaneous change with the level of irradiation, starting from 25°C and then returning to approximately 26°C. An increase in irradiation is associated with an increase in temperature. Physically, an increase in irradiation also results in increased heating on the PV surface. However, an increase in temperature has a detrimental effect on the V_{oc} of the PV module. As the temperature rises, the voltage decreases, thereby allowing the MPP point to shift towards a lower voltage, despite the total power increasing due to the rise in current. Thus, the combination of changes in irradiation and temperature causes the MPP to move dynamically in the V–P plane, which is the basis for the evaluation of the effectiveness of the MPPT algorithm being tested.

Fig. 8 illustrates the results of the PV output power for the four algorithms under comparison, including P&O, InC, H-POnIC, and HI-POnIC. Within the initial time range (0–10s), as irradiation conditions gradually increased, all four algorithms exhibited an ability to effectively follow the power changes, albeit with varying levels of oscillation. The most noticeable change around the MPP point was in P&O. This is because this method exclusively examines changes in ΔP and ΔV, not the actual gradient. In contrast, InC exerted a more stable response as it used a differential approach (dI/dV) to find the MPP position. H-POnIC, a combination of the two, facilitates a more rapid transition than pure InC. However, minor changes were observed due to the weights in the ΔD_{po} and ΔD_{inc} fusion processes were fixed.

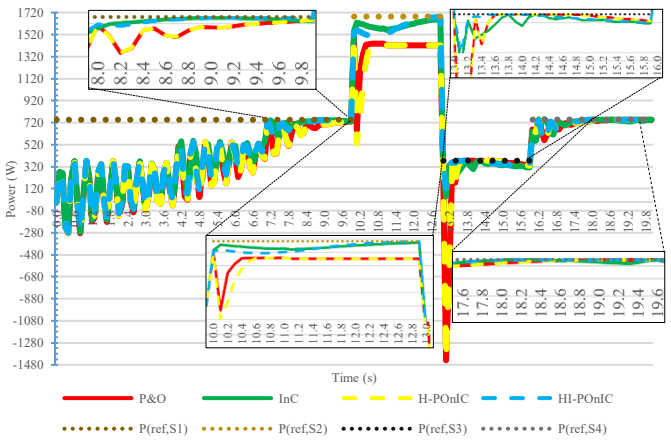

Fig. 8. Results of the real-time dynamic testing on the PV module

During the period of sharp decrease in irradiance (t≈13s), both P&O and H-POnIC exhibited substantial transient deviations, with some samples even producing momentary negative power values. It should be emphasized that this negative power is atypical in the context of PV operation and is not interpreted as the physical behavior of the module absorbing power. This phenomenon is more consistent with a computational artifact resulting from the asynchrony of voltage and current sampling at microsecond time resolution, as well as DC–DC converter transients when the duty cycle changes rapidly. Under rapid change conditions, V and I may be sampled at different effective times (sample skew), resulting in the instantaneous power multiplication ($P = V \cdot I$) not representing a physically coherent pair of V and I. Furthermore, switching transients can also cause temporary overshoot or undershoot prior to the system attaining a new steady state.

HI-POnIC algorithm exhibits optimal performance, characterized by rapid convergence, minimal overshoot, and rapid adaptation following substantial irradiation changes at

approximately t = 13 s. This phenomenon arises because, in the HI-POnIC algorithm, the combination weights ω_{po} and ω_{inc} are calculated adaptively based on Eq. (14) and (15). This enables the system to adjust the contribution of both methods in accordance with changing conditions. It demonstrates the improved transient response and adaptive stability that are fundamental to the novelty of this method. It is supported by the fact that every design in reasonable adaptive control will produce a faster response, higher stability, consideration of transient limits, and adaptive system stability [32–34]. Travis et al. and Yang et al. revealed that adaptive control is capable of improving both the stability and transient performance of the system [35,36]. Wang also emphasized that the aspects of fast response and adaptive stability are fundamental [37].

3.2. Tracking efficiency and power loss

Tracking efficiency in this study is defined based on integrated energy throughout the testing interval. This is measured as the ratio between the energy generated by the MPPT algorithm (E_o) and the maximum reference energy from the MPP model (E_{ref}) at the same irradiance and temperature profiles. This energy-based approach assesses performance more realistically under dynamic conditions as it directly quantifies the impact of oscillations and response delays on the total energy that is successfully extracted. Integrated energy efficiency measurements aim to reveal aspects of operational efficiency and energy optimization [38]. The following equation demonstrates integrated energy-based output efficiency (η).

$$\eta = \frac{E_o}{E_{ref}} x100\% \tag{21}$$

Meanwhile, energy loss (L) is the area between the reference power ($P_{ref}(t)$) and the algorithm power ($P_{alg}(t)$) and can be defined as follows.

$$L = \int max\left(0, P_{ref}(t) - P_{alg}(t)\right) dt \tag{22}$$

Under STC conditions, as depicted in Table 2, HI-POnIC produces the highest energy tracking efficiency and lowest energy loss in comparison to the other algorithms. This interpretation is consistent with the adaptive weighting mechanism and correction steps that enable balancing transient convergence speed and steady-state stability [24]. The adaptive weighting component based on dynamic indicators in HI-POnIC provides significant advantages in damping oscillations and accelerating system stability.

Table 2. Power efficiency in STC environments

Algorithm	Transient Phase ($t \leq 6.5s$)			Steady-State Phase ($t > 6.5s$)		
	Eo (J)	η (%)	L (J)	Eo (J)	η (%)	L (J)
P&O	60.43	80.49	14.781	70.12	93.33	4.97
InC	62.82	83.67	12.399	72.99	97.19	2.10
H-POnIC	60.46	80.52	14.757	71.08	94.66	4.01
HI-POnIC	72.89	97.07	2.196	74.28	98.93	0.81

Further analysis in Tables 3 and 4 demonstrates the system's response to dynamic conditions representing variations in irradiance and temperature. $\eta_{\mathrm{P\&O}}$ and $L_{\mathrm{P\&O}}$ representing efficiency and power loss, respectively, are measured using the P&O method. η_{InC} and L_{InC} are analyzed using the InC method, $\eta_{\mathrm{H-POnIC}}$ and $L_{\mathrm{H-POnIC}}$ are evaluated using the H-POnIC method. Finally, $\eta_{\mathrm{HI-POnIC}}$ and $L_{\mathrm{HI-POnIC}}$ are evaluated using the HI-POnIC method. The measurement results of η and L indicate that HI-POnIC can maintain an average efficiency of 97.52% with a power loss of 2.48 J. This suggests that its adaptive mechanism can adapt in real-time to environmental changes without causing significant deviations. In contrast, the P&O and InC algorithms exhibit a decrease in efficiency to 63–71%, particularly during high irradiation fluctuations (S3), due to oscillatory responses and errors in power gradient direction. This finding demonstrates that the superiority of HI-POnIC is not only nominal, but also that its structure is capable of simultaneously balancing responsiveness and stability. The identification of energy losses is of crucial as part of energy efficiency efforts in the power generation and distribution industry [39]. Accurate measurement of losses is also necessary in PV system design to achieve optimal electrical power [40].

Table 3. Power efficiency when applied in real-time

Time Segment	$\eta_{\mathrm{P\&O}}$ (%)	η_{InC} (%)	$\eta_{\mathrm{H-POnIC}}$ (%)	$\eta_{\mathrm{HI-POnIC}}$ (%)
S1 (0-10s)	63.88	70.02	63.90	94.21
S2 (10-13s)	75.81	71.52	75.98	97.78
S3 (13-16.5s)	37.57	42.62	37.62	66.27
S4 (16.5-20s)	61.79	67.79	61.84	92.60

Table 4. Power loss when real-time is applied

Time Segment	$L_{\mathrm{P\&O}}$ (J)	L_{InC} (J)	$L_{\mathrm{H-POnIC}}$ (J)	$L_{\mathrm{HI-POnIC}}$ (J)
S1 (0-10s)	19.85	16.44	19.84	5.79
S2 (10-13s)	13.03	12.73	12.95	2.22
S3 (13-16.5s)	14.23	13.09	14.22	33.73
S4 (16.5-20s)	14.46	12.22	14.44	7.40

Most MPPT literature evaluates tracking efficiency based on the power generated under steady-state conditions around the maximum power point [18,19,41–44]. To facilitate a fair comparison with these comparative methods, this study also presents a steady-state power efficiency analysis calculated at specific time intervals when the system has reached steady-state conditions. As demonstrated in Fig. 8, steady-state conditions are identified in four times segments, which are S1 (8.7–9.9 s), S2 (11.9–12.9 s), S3 (15–16 s), and S4 (18–20 s). The power efficiency value is calculated as the average power in each of these time segments and is used as the basis for comparing steady-state power efficiency between algorithms.

These measurement results are summarized in Table 5, where η_{ss} represents steady-state power efficiency, while η_{ssi} indicates power efficiency in each time segment (S_i). To observe the clarity of power efficiency in each time segment in the HI-POnIC algorithm, the η_{ssi} values are displayed sequentially from S1 to S4 to ascertain the consistency of

power efficiency under various steady-state operating conditions.

Table 5. Sum. of power efficiency and energy loss when real-time is applied

Algorithm	η_{ss} (%)	η_{ssi}(%)
HI-POnIC	98.69	99.84
		99.65
		95.46
		99.83
Hybrid P&O and InC [18]	85.60	
GSA–PSO Based MPPT [19]	95.50	
P&O with SEPIC Topolgy [41]	95	
ANN-PSO[42]	67	
InC with Constant Irradiance [43]	97	
PnO with Constant Irradiance [43]	94	
ABC [44]	97.68	

As illustrated in Table 5, the steady-state power efficiency of various MPPT methods is highly dependent on the employed control mechanism, the sensitivity to changes in operating conditions, and the characteristics of the utilized converter. Conventional methods, such as P&O with SEPIC topology and P&O/InC, can achieve relatively high efficiency (94–97%) under constant irradiance conditions. However, these results are largely obtained under ideal steady-state conditions and are sensitive to residual oscillations around the MPP [41,43]. It is in line with the basic characteristics of P&O and InC, which employ fixed perturbation steps or local gradient estimation. Consequently, when confronted with more complex irradiance dynamics, the system exhibits a decreased performance.

Artificial intelligence-based approaches and global optimization, such as ANN-PSO and GSA–PSO-based MPPT, exhibit wider efficiency variations [19,42]. While these methods are theoretically capable of identifying the global maximum power point, steady-state performance is significantly influenced by the quality of training, optimization parameters, and computational complexity. In practice, dependence on the learning process and global iterations can result in efficiency degradation when operating conditions deviate from those assumed during the design or training stages, as reflected in lower η_{ss} values [42].

Conventional hybrid methods, such as Hybrid P&O–InC, have successfully enhanced efficiency when compared to single methods by combining the response speed of P&O with the sensitivity of InC gradients. However, this approach generally relies on a static control structure, which limits its ability to adaptively balance transient response and steady-state stability across the entire range of operating conditions. Consequently, the efficiency achieved is in the mid-range (85–95%) and still exhibits power oscillations around the MPP [18].

In this context, the proposed HI-POnIC algorithm achieves the highest steady-state efficiency (98.69%) with consistently high efficiency values across all time segments. This advantage does not stem from an increase in instantaneous power; rather, it is the result of the algorithm's ability to maintain stable operation near the MPP during steady-state intervals. This is achieved through an adaptive weighting mechanism and variable control steps based on local dynamic indicators. In contrast to AI-based or metaheuristic methods, HI-POnIC does not rely on data learning or global search processes. Instead, it applies deterministic decision rules that adjust the contribution of P&O and InC contextually. This approach allows high efficiency to be achieved with low computational complexity and greater stability, making it more relevant for real-time implementation in PV systems.

3.3. Spatial analysis and power tracking accuracy statistics

Spatial and statistical analyses are presented to assess the algorithm's ability to follow the maximum power point under various environmental conditions. To compare the proposed algorithm to conventional methods, three-dimensional visualization and error distribution are utilized to ascertain the accuracy and consistency of the former.

3.3.1. HI-POnIC algorithm performance

To assess the performance of the proposed algorithm in greater depth, a visual analysis was conducted on the relationship between irradiance, temperature, and output power. The subsequent four panels provide a comprehensive depiction of the HI-POnIC algorithm.

Fig. 9 illustrates the mapping of the relationship between irradiance, temperature, and the power output of the PV system controlled by the HI-POnIC algorithm. This is compared to the MPP reference model. The upper left panel displays the reference power surface, which demonstrates that an increase in irradiance consistently increases the maximum power. Conversely, a modest increase in temperature results in a decrease in output, as elevated temperatures have a negative effect on the efficiency of PV cells. The upper right panel displays the empirical surface of the HI-POnIC algorithm. While a parallel trend is evident, disparities emerge in the areas characterized by elevated irradiance and medium temperature. The bottom left panel displays an error surface map that illustrates the power difference between reference and algorithm results. This difference is examined more closely. The presence of smooth gradient color pattern indicates that the error is minimal and consistent under most operating conditions. The presence of small positive values in the low irradiance region indicates the algorithm can respond immediately to changes in light intensity. The bottom right panel displays an overlay between the reference model and the algorithm results, showing that the two surfaces almost overlap. This finding indicates that the HI-POnIC algorithm can replicate the characteristics of the reference model with minimal deviation.

3.3.2. Error performance evaluation

As a quantitative performance evaluation measure, Error Surface analysis is utilized to evaluate the capacity of each algorithm to follow the reference maximum power model under various combinations of irradiance and temperature. In addition, it is employed to map the distribution of power deviation from the ideal MPP conditions.

As depicted in Fig. 10, all algorithms demonstrate a

tendency for error to decrease as irradiance increases, albeit with varying degrees of stability. The P&O and InC algorithms demonstrate more uneven color variations, indicating error fluctuations within the medium irradiance range. The conventional P&O and InC algorithms demonstrate a greater variability in errors with uneven gradations, suggesting fluctuations in deviation from high irradiance conditions. However, H-POnIC can show a stable and concentrated error distribution in the low range. This finding indicates that H-POnIC is regarded capable of tracking MPP stably and consistently. In contrast, the HI-POnIC algorithm yields the optimal results. The analysis reveals that blue is the predominant color in the G–T range, indicating that power deviation is low below 50 W. This observation confirms the efficacy of the AI-inspired adaptation mechanism in HI-POnIC in suppressing error fluctuations, enhancing tracking accuracy, and strengthening the system's resilience to environmental variations.

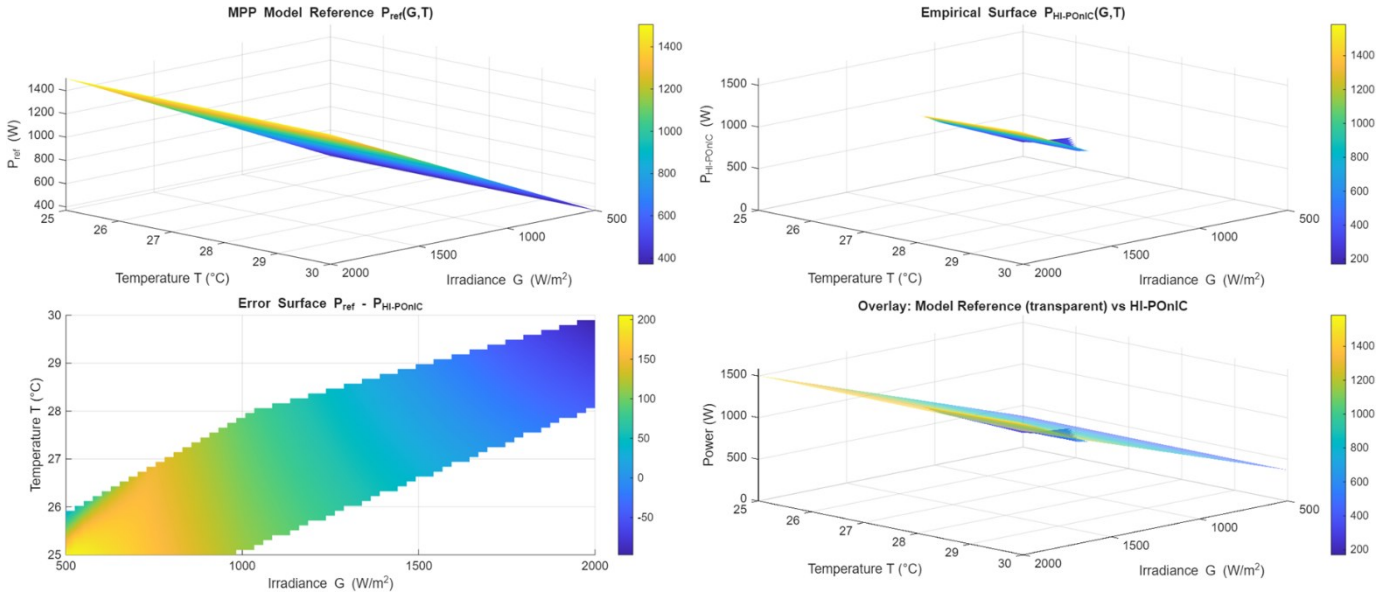

Fig. 9. Spatial analysis of HI-POnIC algorithm performance

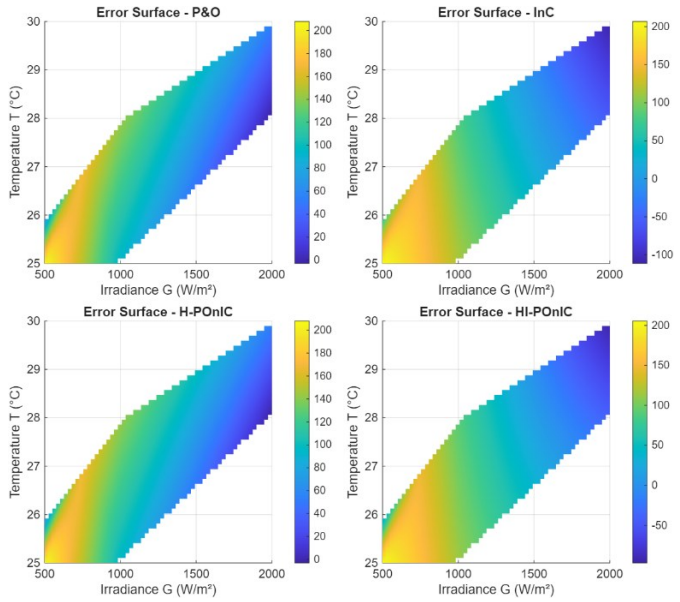

Fig. 10. Error performance analysis

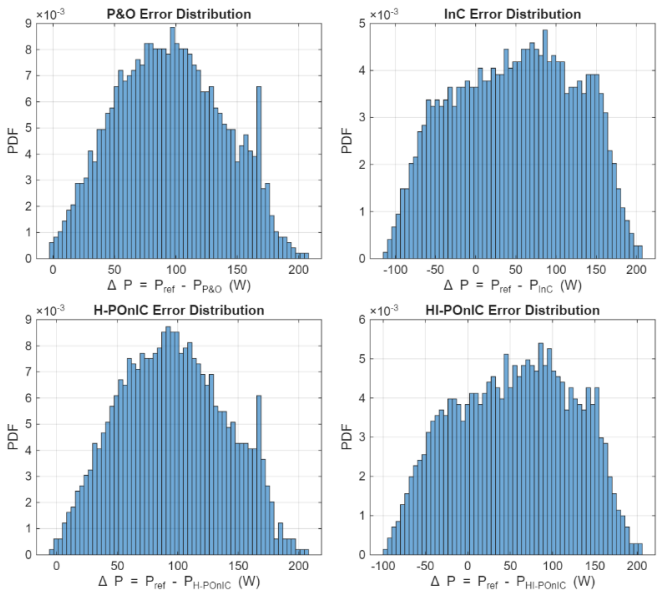

Fig. 11. Power error distribution analysis

3.3.3. Power error distribution

To examine the deviations of each algorithm from the MPP reference model, the power error distribution measure is employed. This measure helps to illustrate the statistical aspects associated with the stability and consistency of each algorithm's accuracy in tracking power under various environmental conditions.

As illustrated in Fig. 11, the P&O and InC algorithms exhibit a broader spectrum of errors. This results in a more dispersed distribution of errors, leading to a diminished stability of the tracking response when the temperature and irradiance change. In contrast, the H-POnIC algorithm demonstrates a narrower distribution with a peak around ΔP≈80-100 W, indicating better accuracy when compared to conventional methods. The HI-POnIC error distribution is even more centered and symmetrical with a higher density peak, indicating minor and

more consistent power errors. It is also supported by the fact that errors symmetrical about zero and with a mode near zero indicate that the difference between the predicted value and the actual value is close to zero, thereby signifying high degree of model accuracy [45,46]. The Probability Density Function (PDF) scale is utilized to indicate the frequency or likelihood of the error occurring.

Quantitatively, the error distribution can be illustrated through the Mean Absolute Error (MAE) statistical value, which represents the average absolute error between the P_{ref} and P_{alg} values, as shown in the following Eq. (23) [47]. MAE serves to evaluate the overall accuracy of the algorithm without overemphasizing significant errors.

$$MAE = \frac{1}{N}\sum_{i=1}^{N}\left|P_{ref,i} - P_{alg,i}\right| \quad (23)$$

The error distribution can also be illustrated through the Mean Squared Error (MSE) using the Root Mean Squared Error (RMSE) formula, as demonstrated in the following Eq. (24) [47]. In contrast to MAE, RMSE is more sensitive to significant errors, because the errors are squared before being summed. The RMSE function is used to check a stable system and to show the significant changes affecting it.

$$RMSE = \sqrt{\frac{1}{N}\sum_{i=1}^{N}\left(P_{ref,i} - P_{alg,i}\right)^2} \quad (24)$$

To normalize the MAE and RMSE values against the reference, Normalized MAE (nMAE) and nRMSE are formed using the following Eq. (25-26).

$$nMAE = \frac{MAE}{P_{ref,max}} x100\% \quad (25)$$

$$nMRSE = \frac{RMSE}{P_{ref,max}} x100\% \quad (26)$$

nMAE is formed to facilitate comparisons between algorithms in PV systems with different power scales. Concurrently, nRMSE is employed to demonstrate the relative stability of the algorithm in percentage form under operating conditions. The results of the calculations in Eq. (23-26) are presented in Table 6.

Table 6. Error distribution statistics against reference power values

Algorithm	MAE (W)	RMSE (W)	nMAE (%)	nRMSE (%)
P&O	95.695	105.063	10.03	11.01
InC	74.162	89.049	7.77	9.33
H-POnIC	95.828	105.188	10.04	11.02
HI-POnIC	52.965	60.802	3.45	3.96

As depicted in Table 6 the MAE and RMSE values for the P&O and InC methods remain reasonably high. This indicates that they are not operating at their maximum power point. It is evident that H-POnIC has not had significant enhancement, as its adjustment weights remain unaltered. In contrast, the HI-POnIC algorithm exhibits the most significant decline in error, with a nMAE of 3.45% and a nRMSE of 3.96%. This demonstrates that adaptive mechanisms, akin to AI, can ensure the accuracy and stability of power tracking, even in fluctuating temperature and irradiance. The MAE and RMSE numbers are more reliable because they are easily comprehensible and can be applied in real life scenarios. This renders them more beneficial for those endeavoring to conceptualize and design a system [48].

4. Conclusion

This study effectively introduced the HI-POnIC algorithm as an adaptive evolution of the integration of the P&O and InC methodologies. The HI-POnIC algorithm is designed without involving learning models or training processes. Instead, it utilizes a deterministic adaptive decision mechanism based on system features. This mechanism allows control responses to be adjusted in accordance with changes in the operating characteristics of photovoltaic modules. The findings of the test demonstrated that HI-POnIC exerted faster convergence time and enhanced stability around the maximum power point when compared to conventional methods. The employment of dynamic weighting and adaptive steps enabled HI-POnIC to balance transient response and steady-state stability, thereby suppressing oscillations and power loss without increasing computational complexity or dependence on training parameters.

Integrated assessments of energy efficiency and power efficiency under steady-state conditions exhibited uniform performance across a broad spectrum of irradiance and temperature fluctuations. The lightweight and fully deterministic implementation characteristics of this approach have the potential to be further developed for more complex PV systems and multi-input renewable energy systems. This would improve the flexibility and performance of maximum power tracking in increasingly diverse environmental conditions.

Acknowledgements

The author(s) disclosed receipt of the following financial support for the research, authorship, and/or publication of this article: This work was supported by the Politeknik Negeri Jakarta [grant numbers 218/PL3.A.10/PT.00.06/2025].

References

1. IEA, *Global share of electricity generation, 2019 – Charts – Data & Statistics*, IEA. 2020.
2. K SB, M Y, *Coal Fired Power Plants: Emission Problems and Controlling Techniques*, J. Earth Sci. Clim. Change. 8 (2017) 1–9.
3. Kumar S, Sadeq A, *Renewable Energy Systems*, 2024.
4. *Energy | Department of Economic and Social Affairs*, 2025.
5. Kannan N, Vakeesan D, *Solar energy for future world: - A review*, Renew. Sustain. Energy Rev. 62 (2016) 1092–105.
6. Pusch A, Römer U, Culcer D, Ekins-Daukes NJ, *Energy Conversion Efficiency of the Bulk Photovoltaic Effect*, PRX Energy. 2 (2023) 013006.
7. Lüer L, Peters IM, Corre VML, Forberich K, Guldi DM, Brabec CJ, *Bypassing the Single Junction Limit with Advanced Photovoltaic Architectures*, Advanced Materials. 36 (2025).
8. Dada M, Popoola P, *Recent advances in solar photovoltaic materials and systems for energy storage applications: a review*, Beni-Suef Univ. J. Basic Appl. Sci. 12 (2023) 1–15.
9. Hossain MJ, Sun M, Davis KO, *Photon management in silicon photovoltaic cells: A critical review*, Sol. Energy Mater. Sol. Cells. 267

(2024) 112715.
10. Muldarisnur M, Fahendri F, Perdana I, Abdullah Z, Yusfi M, *Light absorption enhancement in organic solar cell using non-concentric Ag:SiO2 core-shell nanoparticles*, Communications in Science and Technology. 8 (2023) 50–6.
11. Tofigh Rihani A, Ghandchi M, *Increasing the Efficiency of Photovoltaic Systems by Using Maximum Power Point Tracking (MPPT)*, J. Artif. Intell. Electr. Eng. 4 (2015) 45.
12. Verma D, Nema S, Shandilya AM, Dash SK, *Maximum power point tracking (MPPT) techniques: Recapitulation in solar photovoltaic systems*, Renew Sustain Energy Rev. 54 (2016) 1018–34.
13. Haque A, *Maximum Power Point Tracking (MPPT) Scheme for Solar Photovoltaic System*, Energy Technol. Policy. 1 (2014) 115–22.
14. Samosir AS, Gusmedi H, Purwiyanti S, Komalasari E, *Modeling and Simulation of Fuzzy Logic based Maximum Power Point Tracking (MPPT) for PV Application*, Int. J. Electr. Comput. Eng. 8 (2018) 1315–23.
15. Ali A, Hasan AN, Marwala T, *Perturb and observe based on fuzzy logic controller maximum power point tracking (MPPT)*, In: 2014 International Conference on Renewable Energy Research and Application (ICRERA). Milwaukee, WI, USA, 2014, pp. 406–11.
16. Ahmed J, Salam Z, *A Maximum Power Point Tracking (MPPT) for PV system using Cuckoo Search with partial shading capability*, Applied Energy. 119 (2014) 118–30.
17. Yüksek G, Mete AN, *A hybrid variable step size MPPT method based on P&o; INC methods*, In: 2017 10th International Conference on Electrical and Electronics Engineering (ELECO). Bursa, Turkey, IEEE 2017, pp. 949–53.
18. Buch K, Bhatt C, Patel U, Tekwani PN, *A Novel Hybrid MPPT Technique for PSC using Weighted Average Approach*, In: 2023 IEEE Texas Power and Energy Conference (TPEC). College Station, TX, USA, 2023, pp. 1–6.
19. Priyadarshi N, Bhaskar MS, Padmanaban S, Blaabjerg F, Azam F, *New CUK–SEPIC converter based photovoltaic power system with hybrid GSA–PSO algorithm employing MPPT for water pumping applications*, IET Power Electronics. 13 (2020) 2824–30.
20. Fahim SR, Hasanien HM, Turky RA, Aleem SHEA, Ćalasan M, *A Comprehensive Review of Photovoltaic Modules Models and Algorithms Used in Parameter Extraction*, Energies. 15 (2022) 8941.
21. Stanojević M, Gojanović J, Matavulj P, Živanović S, *Organic solar cell physics analyzed by Shockley diode equation*, Opt Quant Electron. 52 (2020) 345.
22. Katche ML, Makokha AB, Zachary SO, Adaramola MS, *A Comprehensive Review of Maximum Power Point Tracking (MPPT) Techniques Used in Solar PV Systems*, Energies. 16 (2023) 2206.
23. Safari A, Mekhilef S, *Simulation and Hardware Implementation of Incremental Conductance MPPT With Direct Control Method Using Cuk Converter*, IEEE Trans. Ind. Electron. 58 (2011) 1154–61.
24. Irijanti E, *Modified Adaptive Support Weight for Stereo Matching*, Communications in Science and Technology. 2 (2017).
25. Badan Pengkajian dan Penerapan Teknologi, *Test Report BPPT SLX-375-72M Monocrystalline*, Tangerang Selatan, Indonesia: The Natıonal Research And Innovatıon Agency (BRIN) 2021. Report No.: 012/LAP.JATEK/B2TKE/BPPT/III/2021.
26. Kabalan A, Jiorle C, Abouelnagga A, *A Real-Time Monitoring Device for Assessing Photovoltaic Performance in Residential Settings*, Electronics. 14 (2025) 3771.
27. Singh YK, Dubey S, Rajput P, Singh KY, Pandey K, *Real-time and modelled performance assessment and validation studies of PV modules operating in varied climatic zones*, Energy Built. Environ. 6 (2025) 585–95.
28. Razak A, Irwan YM, Leow WZ, Irwanto M, Safwati I, Zhafarina M, *Investigation of the Effect Temperature on Photovoltaic (PV) Panel Output Performance*, Int. J. Adv. Sci. Eng. Inf. Technol. 6 (2016) 682–8.
29. Han JY, Li SY, *Impact of temperature and solar irradiance in shadow covering scenarios via two-way sensitivity analysis for rooftop solar photovoltaics*, Energy Sources Part A Recovery Util. Environ. Eff. 46 (2024) 3165–76.
30. Li Z, Yang J, Dezfuli PAN, *Study on the Influence of Light Intensity on the Performance of Solar Cell*, Int. J. Photoenergy. 2021 (2021) 6648739.
31. Ryu S, Ha NY, Ahn YH, Park JY, Lee S, *Light intensity dependence of organic solar cell operation and dominance switching between Shockley–Read–Hall and bimolecular recombination losses*, Sci. Rep. 11 (2021) 16781.
32. Humaidi AJ, Hameed AH, *Design and Comparative Study of Advanced Adaptive Control Schemes for Position Control of Electronic Throttle Valve*, Information. 10 (2019) 65.
33. Cao C, Hovakimyan N, *Design and Analysis of a Novel \cal L_1 Adaptive Control Architecture With Guaranteed Transient Performance*, IEEE Trans. Autom. Control. 53 (2008) 586–91.
34. Hansen J, Johansen TA, *Transient performance, resetting and filtering in nonlinear multiple model adaptive control*, In: Proceedings of the 2004 American Control Conference. 2004, pp. 1223–8 vol.2.
35. Gibson TE, Annaswamy AM, Lavretsky E, *Adaptive Systems with Closed–loop Reference Models: Composite control and observer feedback*, IFAC Proc. Vol. 46 (2013) 440–5.
36. Yang J, Na J, Gao G, *Robust model reference adaptive control for transient performance enhancement*, Int. J. Robust Nonlinear Control. 30 (2020) 6207–28.
37. Wang QG, Sun J, Zhang JX, Huang J, Yu J, Dong H, *Survey of transient performance control*, Control Eng. Pract. 138 (2023) 105559.
38. Shame BH, Ubaidillah, Tjahjana DDDP, Arifin Z, Aziz M, Harwijayanti W, et al., *The renewable energy research contribution of Tanzania: A review*, Communications in Science and Technology. 9 (2024) 65–86.
39. Masoomi M, Panahi M, Moradihamedani A, *Energy-saving mechanisms for evaluating efficiency improvement and losses reduction scenarios in the thermal power plants sector of Iran*, Energy Sources Part B Econ. Plan. Policy. 18 (2023) 2215260.
40. Bruno JC, Pulido T, *Review and Analysis of Energy Losses and Inverter Sizing in Photovoltaic Plants*, Rochester, NY: Social Science Research Network 2024.
41. Widjonarko, Bukhori S, Pratama AP, *An Improving Efficiency MPPT in PV Systems with a Modified Voltage Regulator*, In: 2021 International Seminar on Intelligent Technology and Its Applications (ISITIA). Surabaya, Indonesia, 2021, pp. 179–83.
42. Hamzah M ilham hasby, Aprillia H, Giyantara A, *Hybrid ANN-PSO Based MPPT Optimization for Enhanced Solar Panel Efficiency*, ELKHA J. Tek. Elektro. 17 (2025) 32–7.
43. Abdulrazzaq AA, Ali AH, *Efficiency Performances of Two MPPT Algorithms for PV System With Different Solar Panels Irradiancess*, Int. J. Power Electron. Drive Syst. 9 (2018) 1755–64.
44. Priyadarshi N, Padmanaban S, Holm-Nielsen JB, Bhaskar MS, Azam F, *Internet of things augmented a novel PSO-employed modified zeta converter-based photovoltaic maximum power tracking system: hardware realisation*, IET Power Electron. 13 (2020) 2775–81.
45. Yannick TL, Juste Constant EE, Pierre Boris Gael E, Andre William B, Luc Leroy MN, Arlin Bruno T, et al., *Durability, thermo-physical characteristics, and mechanical strength prediction of green Portland cement matrix incorporating recycled soda-lime glass and lead glass*, Heliyon. 10 (2024) e26288.
46. Boroh AW, Kouayep Lawou S, Mfenjou ML, Ngounouno I, *Comparison of geostatistical and machine learning models for predicting geochemical concentration of iron: case of the Nkout iron deposit (south Cameroon)*, J. Afr. Earth Sci. 195 (2022) 104662.
47. Hodson TO, *Root-mean-square error (RMSE) or mean absolute error (MAE): when to use them or not*, Geosci. Model Dev. 15 (2022) 5481–7.
48. Khoshvaght H, Permala RR, Razmjou A, Khiadani M, *A critical review on selecting performance evaluation metrics for supervised machine learning models in wastewater quality prediction*, J. Environ. Chem. Eng. 13 (2025) 119675.